ChemComm

COMMUNICATION

In situ quantitation of intracellular microRNA in the whole cell cycle with a functionalized carbon nanosphere probe†

Xianjiu Liao and Huangxian Ju*

Cite this: *Chem. Commun.*, 2015, **51**, 2141

Received 14th November 2014,
Accepted 19th December 2014

DOI: 10.1039/c4cc09097g

www.rsc.org/chemcomm

A method was designed for *in situ* quantitation and monitoring of the change in intracellular microRNA in the whole cell cycle with a functionalized carbon nanosphere probe.

MicroRNAs (miRNAs) are a group of non-coding, endogenous and small-sized RNAs. They play significant regulatory roles in a wide variety of biological processes including cell development, differentiation, metabolism, and apoptosis.[1] Specifically, the aberrant expression and misregulation of miRNAs can lead to various diseases.[2] Therefore, miRNAs have been recognized as a clinically important class of diagnostic and prognostic biomarkers and reliable indicators of the cellular status,[3] and their detection has formed a rapidly emerging field for further understanding the biochemical function of miRNAs and exploring useful diagnostic and prognostic markers of diseases. Many techniques such as real-time quantitative PCR,[4] northern blotting[5] and microarrays[6] have been extensively used for miRNA analysis.[7] However, these techniques need a miRNA isolation step for sample preparation, the *in situ* monitoring of miRNAs in living cells is still a challenge.

Intracellular miRNAs can affect the growth of cancer cells by regulating cell cycle control factors.[8] The optimal understanding of the roles of miRNAs in the cell cycle and the miRNA related cell cycle bioprocesses relies on the development of methodology for detecting the miRNA expression levels in the whole cell cycle of living cells. Thus it is an urgent demand to develop reliable miRNA sensing platforms for *in situ* monitoring the change in intracellular miRNAs in the whole cell cycle.

Some confocal imaging methods have been developed for monitoring intracellular functional biomolecules.[9] Our previous studies also proposed some confocal imaging methods for detection of intracellular miRNA and telomerase.[10] Recently carbon nanospheres (CNSs) have been reported to possess high chemical stability, convenient and green preparation, high water dispersibility and good biocompatibility.[11] Therefore, this work used CNSs as a novel nanocarrier to deliver a gene probe into cells for the design of an intracellular miRNA detection strategy.

Single-stranded DNA (ssDNA) can conveniently be assembled on CNSs through their strong π–π interaction. Similar to graphene oxide,[12] CNSs can act as a fluorescence (FL) quencher of dye-labeled ssDNA assembled on their surface,[13] and the hybridization of the adhered ssDNA with a complementary target weakens the π–π interaction between bases and CNSs, which leads to the release of the adhered ssDNA from the CNSs and the recovery of dye FL.[12a,13] Moreover, folic acid as a generally used cancer cell-target-specific moiety[14] can also be conveniently assembled on CNSs through its π–π interaction with carbon structure.[15]

In view of the advantages of CNSs, this work developed a confocal imaging method for target-cell-specific quantitation of intracellular miRNA by co-assembling folic acid (FA) and cyanine dye 5 (Cy5)-labeled ssDNA (Cy5-ssDNA) on the CNS surface (Scheme 1). Using miRNA-18a as an analyte model, this work further transfected miRNA-18a mimic into the cells synchronized at different phases to obtain the calibration curves and proposed a quantitative method for detection of intracellular miRNA in the whole cell cycle. The results demonstrated that the

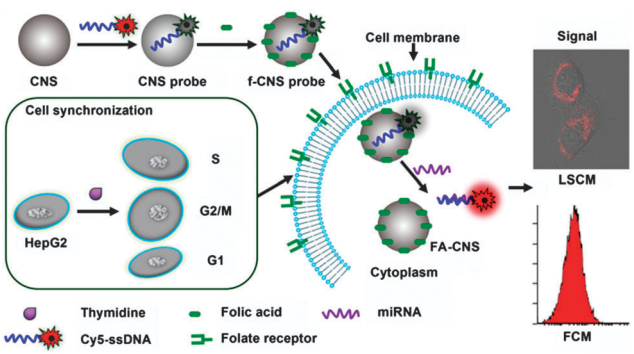

Scheme 1 Schematic illustration of f-CNS probe preparation and *in situ* intracellular detection of miRNA in the whole cell cycle by confocal imaging and flow cytometric analysis using the f-CNS probe.

State Key Laboratory of Analytical Chemistry for Life Science, School of Chemistry and Chemical Engineering, Nanjing University, Nanjing 210093, P. R. China. E-mail: hxju@nju.edu.cn; Fax: +86 25 83593593; Tel: +86 25 83593593

† Electronic supplementary information (ESI) available: Experimental details and additional figures. See DOI: 10.1039/c4cc09097g

proposed cell-target-specific delivery and detection system would be attractive for the study of miRNA related cell cycle bioprocesses and clinic biomedical application.

Both the bare CNSs and f-CNS probe showed a narrow size distribution with an average diameter of about 120 nm and 125 nm (Fig. S1, ESI†), respectively. The 5 nm change of DLS diameter resulted from the presence of Cy5-ssDNA and folic acid on f-CNS and their different charge distribution. Relative to bare CNSs (Fig. S2A, ESI†), the SEM image of the f-CNS probe showed an island structure (Fig. S2B, ESI†), indicating that dense ssDNA and FA were loaded on the surface of CNSs. The FT-IR spectrum indicated the existence of –OH and –COOH groups and the formation of hydrogen bonding between –OH or –COOH groups of CNSs and –OH, –COOH or $-NH_2$ groups of the FA (Fig. S2C, ESI†), which strengthened the stability of FA-CNSs.[16]

The presence of –OH and –COOH groups on the CNS surface led to a negative zeta potential of −14.6 mV (Fig. S2D, ESI†). After ssDNA was assembled on CNSs, the zeta potential became more negative due to the negatively-charged phosphate of ssDNA. The FA made the zeta potential of f-CNS probe more negative. The change in zeta potential confirmed the successful preparation of the f-CNS probe.

To confirm the feasibility of the designed method, the FL quenching ability of CNSs and the release of Cy5 labeled DNA strand from the CNSs upon hybridization with miRNA-18a was examined (Fig. 1). After CNS suspension was mixed with Cy5-ssDNA, the FL of Cy5 decreased (Fig. 1A), indicating the quenching effect of CNSs on the FL of Cy5 due to the adsorption of ssDNA on CNSs. The increasing amount of CNSs led to an obvious increase in quenching efficiency. Upon addition of complementary miRNA into the mixture of Cy5-ssDNA and CNSs, the FL of Cy5 could be recovered. The recovery efficiency gradually decreased with the increasing amount of CNSs due to the long-range energy transfer from the dye to the CNSs[17] (Fig. S3A, ESI†). Considering the quenching and recovery efficiency, 120 mg L^{-1} CNSs for 1.0 μM Cy5-ssDNA was selected for the preparation of the f-CNS probe.

After miRNA-18a was added to the suspension of the 120 mg L^{-1} f-CNS probe, the specific recognition of miRNA-18a to Cy5-ssDNA assembled on the f-CNS probe led to the FL recovery due to the formation of a DNA–miRNA duplex helix to weaken the π–π interaction between the bases and CNSs (Fig. 1B). The formation

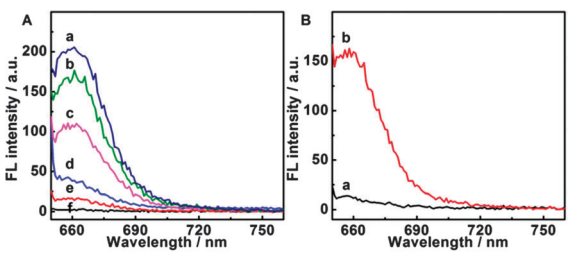

Fig. 1 FL emission spectra of (A) 1.0 μM Cy5-ssDNA after incubation with 0 (a), 20 (b), 60 (c), 100 (d) and 120 mg L^{-1} (e) CNSs for 3 h and 120 mg L^{-1} CNSs as control (f), and (B) 120 mg L^{-1} f-CNS probe (a), 120 mg L^{-1} f-CNS probe after incubated with 6.0 μM target at 37 °C for 1 h (b) in HB. The emission is monitored at 660 nm at 640 nm excitation.

of a Cy5-labeled DNA–miRNA duplex helix was theoretically feasible due to its T_m value of 65.1 °C and the maximum ΔG of −38.77 kcal mol^{-1}, which was calculated with computation of mfold,[18] and could be confirmed using polyacrylamide gel electrophoresis analysis (Fig. S3B, ESI†). It was notable that the CNSs did not exhibit obvious FL emission (Fig. 1A, curve f), suggesting that the interference of CNSs with FL detection was negligible. The proposed system displayed high specificity for discriminating the complementary target from three- and single-base mismatched strands and non-complementary RNA (Fig. S4, ESI†). Thus the designed ''off''–''on'' system possessed a high signal-to-noise ratio for detection of target miRNA-18a.

The ability of CNSs to protect the ssDNA from nuclease cleavage and interfering proteins was confirmed using FL assay (Fig. S5A, ESI†). The protection could be attributed to the shielding from the CNSs or the conformational change of nucleic acid strands when adsorbed on the CNSs surface.[19]

The effect of pH on the stability of the f-CNS probe was also evaluated. The f-CNS probe taken up by cells experienced an increasingly acidic environment as they progressed through the endocytic pathway with a pH change from 4.7 to 8.0.[20] The f-CNS probe showed a negligible FL change at different pH values from 4.0 to 8.0 (Fig. S5B, ESI†), indicating that the f-CNS probe was stable during the endocytic pathway for intracellular transport.

To exactly evaluate the cytotoxicity of gene carrier with MTT assay, the viability of cells transfected with FA-CNSs was compared with those transfected with two commercial transfection agents, Lp2000 and PEI. After HepG2 cells were treated with FA-CNSs from 30 to 360 mg L^{-1} for 3 h, the cells still exhibited the viability from 98.3% to 87.8% (Fig. S6A, ESI†), suggesting that FA-CNSs possessed low cytotoxicity. The viability of cells transfected with 120 mg L^{-1} FA-CNSs was even higher than those transfected with 0.5 mM PEI or 2% Lp2000 (Fig. S6B, ESI†), indicating lower cytotoxicity of the FA-CNSs than Lp2000 and PEI. This could be attributed to the green preparation and negative surface charge of FA-CNSs.[21] The latter lowered the adhesion of FA-CNSs to the cell surface.

The cytotoxicity of FA-CNSs was also studied using Annexin V-FITC/PI-labeling flow cytometric analysis (Fig. S6C, ESI†). In comparison to the control group, both FA-CNSs and Lp2000-transfected cells showed a slightly higher apoptotic rate, which indicated their low cytotoxicity. The apoptotic rate of the cells treated with FA-CNSs was lower than the Lp2000, demonstrating the lower cytotoxicity of CNSs, which was in good agreement with the result of MTT assay. The efficient protection properties, good stability and the lower cytotoxicity of CNSs than commercial transfection agents led to promising application of the probe in *in situ* monitoring of intracellular biomolecules.

The presence of FA achieved the cell-specific delivery of the f-CNS probe into HepG2 cells by its recognition to folate receptor (FR) overexpressed on the cell membrane. With the increasing incubation time of HepG2 cells in f-CNS probe suspension, the transfected cells showed increasing FL (Fig. S7A, column a, ESI†), indicating the increased uptake of f-CNS probe, and reached a plateau at 3.0 h (Fig. S7B, ESI†), which was selected as the optimal incubation time of the f-CNS probe. After HepG2 cells were firstly treated with FA to saturate the FR sites on the cell

surface and then transfected with the f-CNS probe, the cells showed very low FL, which gradually increased with the increasing transfection time (Fig. S7A, column b, ESI†). The FL intensity and its change were similar to those transfected with the CNS probe (Fig. S7A, column c and Fig. S7C, ESI†), indicating the same uptake mechanism, which was different from that of the f-CNS probe into the HepG2 cells. The much higher amount of the f-CNS probe delivered into HepG2 cells supported the specific receptor-mediated endocytosis. The cell specificity of f-CNS probe was further validated using A549 cells (FR-negative cells) and HaCaT cells (non-cancerous cells) as control cell samples, which also showed very low FL (Fig. S7A, columns d and e, ESI†). From the dependence of FL intensity on the amount of f-CNS probe used for transfection of HepG2 cells, the concentration of 120 μg mL^{-1} was selected as the optimal amount of f-CNS probe (Fig. S8, ESI†).

After cellular internalization, the f-CNS probe was delivered to early endosomes, followed by the movement to late endosomes/lysosomes.[22] Thus, the successful endosomal escape of the probe is a critical requirement for miRNA-18a detection. After HepG2 cells were incubated with the mixture of 1.0 μM LysoTracker Green DND-26 and Hoechst 333342 for 20 min, the confocal image showed the endosomes/lysosomes distributed in the cytoplasm[20,23] (Fig. S9A, green, ESI†). The f-CNS probe transfected HepG2 cells also showed strong Cy5 FL in the cytoplasm (Fig. S9B, ESI†), while no obvious Cy5 FL (red) in the cytoplasm could be observed when using the BC-CNS probe to incubate the cells (Fig. S9C, ESI†). Thus both the background interference could be eliminated, and the Cy5 FL resulted from the hybridization of Cy5-labeled DNA assembled on the probe with miRNA-18a in the cytoplasm,[24] which recovered the Cy5 FL.

The efficient endosomal escape of the f-CNS probe could be monitored by incubating the HepG2 cells with the f-CNS probe for different times and then Lysotracker Green DND-26 for 20 min (Fig. S9D-F, ESI†). At a short incubation time of the f-CNS probe, the cells showed little red Cy5 FL. With the increasing incubation time of the f-CNS probe, not only the red Cy5 FL became stronger, but also it separated from the green FL of endosome/lysosome maker, thus more f-CNS probe escaped from endocytic vesicles to recognize miRNA-18a in the cytoplasm, indicating efficient cytoplasmic diffusion of the f-CNS probe.[23,25]

Flow cytometry was used to monitor the cell cycle stage distribution. The unsynchronized cells distributed in three areas (Fig. S10A, ESI†). The first peak with the lowest DNA content represented G1 phase cells, the second peak with the highest DNA content represented G2/M phase cells, and S phase cells located between two peaks. 22.6%, 13.7% and 63.7% of the unsynchronized cells were in S, G2/M and G1 phase, respectively. The low population of S- and G2/M-phase cells should be attributed to their relatively shorter time windows. After the cells were synchronized and released from the block for 4 h, 78.6% of the cells were in S phase (Fig. S10B, ESI†). Further release led to the number increase of G2/M- and G1-phase cells. After release for 8 and 24 h, 64.7% and 79.3% cells progressed to G2/M (Fig. S10C, ESI†) and G1 phase (Fig. S10D, ESI†), respectively, indicating the high synchrony of the cell population. The higher percentage of G1-phase cells at 24 h release resulted from the longer time

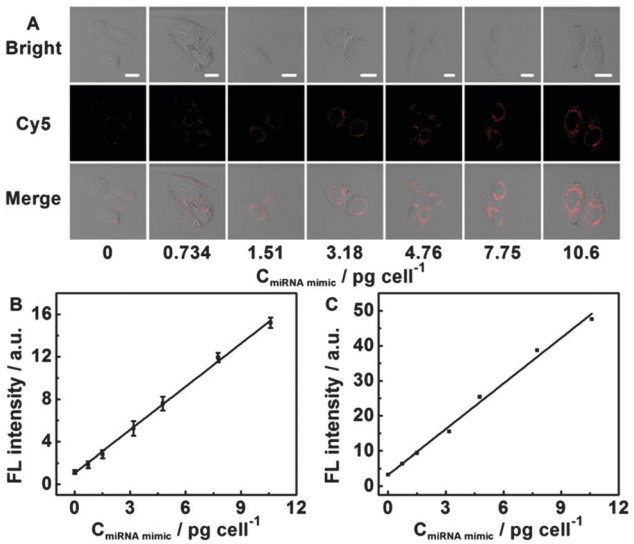

Fig. 2 FL imaging quantitation of intracellular miRNA-18a. (A) FL images of HepG2 cells transfected with different amounts of miRNA-18a mimic for 6 h and then synchronized at S phase to transfect 120 mg L^{-1} f-CNS probe for 3 h at 37 °C. Smart gain: 850 V, scale bars: 20 μm. Plots of mean FL intensities from confocal image (B) and flow cytometric analysis (C) *versus* the quantity of intracellular miRNA-18a mimic.

window of the G1 phase, which also led to the high percentage of the unsynchronized cells at the G1 phase.

To quantitatively detect the amount of miRNA in living cells, 6.8×10^4 HepG2 cells were transfected with different amounts of miRNA-18a mimic, and then synchronized at the S phase and incubated with the f-CNS probe for 3 h to obtain the calibration curve. With the increasing amount of miRNA-18a mimic transfected into a single cell, the confocal microscopic images showed the increasing FL emission (Fig. 2A). The plot of mean FL intensity *versus* the amount of transfected miRNA-18a mimic showed a good linearity (R = 0.999) (Fig. 2B) with a regression equation of $I_{Cy5} = 1.36C_{miRNA\ mimic} + 1.06$. From the slope and the standard deviation for FL measurement of f-CNS probe transfected cells, the detection limit of intracellular miRNA-18a for S-phase HepG2 cells was found to be 0.127 pg $cell^{-1}$. Similarly, the linear regression equations for G2/M- and G1-phase cells were $I_{Cy5} = 1.19C_{miRNA\ mimic} + 1.23$ (R = 0.997) and $I_{Cy5} = 1.31C_{miRNA\ mimic} + 1.61$ (R = 0.999) with the detection limits of 0.172 and 0.152 pg $cell^{-1}$, respectively. Through standard curve extrapolation, the average quantity of miRNA-18a in single S-, G2/M- and G1-phase HepG2 cells was obtained to be 0.779, 1.03 and 1.23 pg, respectively. The S-phase HepG2 cells showed the lowest expression of miRNA-18a, and then rose to higher levels in G2/M and G1 phases, respectively. MiRNA-18a belongs to miRNA-17/20 cluster and can regulate cell cycle progression *via* E2F, c-Myc, Rb and cyclin D1.[8b,26] In HepG2 cells, miRNA-18a is an oncogenic miRNA, and can promote the proliferation and inhibit the death of HepG2 cells.[8c] So, the highest expression of miRNA-18a in the G1 phase may promote G1/S transition and the proliferation of HepG2 cells.

To confirm the detection results with the proposed method, flow cytometric analysis was performed for the detection of intracellular miRNA. The plots of FL intensity *versus* the amount of miRNA-18a mimic in single S- (Fig. 2C), G2/M- and

G1-phase HepG2 cell led to the linear regression equations of $I_{Cy5} = 4.33C_{miRNA\,mimic} + 3.24$ ($R = 0.997$), $I_{Cy5} = 4.26C_{miRNA\,mimic} + 4.13$ ($R = 0.997$) and $I_{Cy5} = 4.33C_{miRNA\,mimic} + 5.25$ ($R = 0.998$), respectively. Thus, the average quantity of miRNA-18a in single S-, G2/M- and G1-phase HepG2 cells was 0.748, 0.969 and 1.21 pg, respectively. The relative deviation between two methods was 4.1%, 6.3% and 1.7%, respectively, indicating good validation of the proposed method.

Using anti-miRNA-18a as an inhibitor to transfect synchronized HepG2 cells, the down-regulation of miRNA-18a level could be monitored with the proposed method. After the cells synchronized at S, G2/M and G1 phase were incubated with anti-miRNA for 48 h, the miRNA-18a level showed 50.6%, 52.0% and 51.5% down-regulation (Fig. S11, ESI†), respectively, which were close to 52.7%, 54.0% and 53.6% down-regulation obtained with flow cytometric analysis. Thus, the proposed method could be used for *in situ* monitoring of intracellular miRNA.

This work designed a f-CNS probe for target-cell-specific quantitation and monitoring of the change in intracellular miRNA in the whole cell cycle. The CNSs show low cytotoxicity and a strong FL quenching effect on the fluorophore, which can be recovered upon the specific recognition of the ssDNA to miRNA. The high FL recovery efficiency, low FL background and good protection properties of CNSs lead to acceptable sensitivity for *in situ* quantitation of intracellular miRNA. Coupled with cell synchronization this proposed method can be used for monitoring the change in intracellular miRNA amount in single cells at different cell phases. The sensing platform for miRNA in the whole cell cycle would be useful for miRNA related investigations.

This research was financially supported by the National Basic Research Program of China (2010CB732400) and the National Natural Science Foundation of China (21135002, 21121091).

Notes and references

1 (*a*) R. H. Plasterk, *Cell*, 2006, **124**, 877–881; (*b*) M. V. Joglekar and V. M. Joglekar, *Gene Expression Patterns*, 2009, **9**, 109–113; (*c*) P. Xu, S. Y. Vernooy, M. Guo and B. A. Hay, *Curr. Biol.*, 2003, **13**, 790–795; (*d*) J. Brennecke, D. R. Hipfner, A. Stark, R. B. Russell and S. M. Cohen, *Cell*, 2003, **113**, 5–36.

2 (*a*) N. Kosaka, H. Iguchi and T. Ochiya, *Cancer Sci.*, 2010, **101**, 2087–2092; (*b*) J. Jiang, E. J. Lee, Y. Gusev and T. D. Schmittgen, *Nucleic Acids Res.*, 2005, **33**, 5394–5403; (*c*) M. A. Lindsay, *Trends Immunol.*, 2008, **29**, 343–351; (*d*) B. R. Cullen, *Genes Dev.*, 2011, **25**, 1881–1894.

3 (*a*) E. Barbarotto, T. D. Schmittgen and G. A. Calin, *Int. J. Cancer*, 2008, **122**, 969–977; (*b*) M. S. Kumar, J. Lu, K. L. Mercer, T. R. Golub and T. Jacks, *Nat. Genet.*, 2007, **39**, 673–677; (*c*) A. Gupta, J. J. Gartner, P. Sethupathy, A. G. Hatzigeorgiou and N. W. Fraser, *Nature*, 2006, **442**, 82–85; (*d*) G. A. Calin and C. M. Croce, *Nat. Rev. Cancer*, 2006, **6**, 857–866; (*e*) C. C. Pritchard, H. H. Cheng and M. Tewari, *Nat. Rev. Genet.*, 2012, **13**, 358–369.

4 (*a*) J. Li, B. Yao, H. Huang, Z. Wang, C. H. Sun, Y. Fan, Q. Chang, S. L. Li, X. Wang and J. Z. Xi, *Anal. Chem.*, 2009, **81**, 5446–5451; (*b*) C. Chen, D. A. Ridzon, A. J. Broomer, Z. Zhou, D. H. Lee, J. T. Nguyen, M. Barbisin, N. L. Xu, V. R. Mahuvakar, M. R. Andersen, K. Q. Lao, K. J. Livak and K. J. Guegler, *Nucleic Acids Res.*, 2005, **33**, e179.

5 (*a*) G. S. Pall, C. Codony-Servat, C. J. Byrne, L. Ritchie and A. Hamilton, *Nucleic Acids Res.*, 2007, **35**, e60; (*b*) S. W. Kim, Z. Li, P. S. Moore, A. P. Monaghan, Y. Chang, M. Nichols and B. John, *Nucleic Acids Res.*, 2010, **38**, e98.

6 P. T. Nelson, D. A. Baldwin, L. M. Scearce, J. C. Oberholtzer, J. W. Tobias and Z. Mourelatos, *Nat. Methods*, 2004, **1**, 155–161.

7 H. F. Dong, J. P. Lei, L. Ding, Y. Q. Wen, H. X. Ju and X. J. Zhang, *Chem. Rev.*, 2013, **113**, 6207–6233.

8 (*a*) F. Fornari, L. Gramantieri, M. Ferracin, A. Veronese, S. Sabbioni, G. A. Calin, G. L. Grazi, C. Giovannini, C. M. Croce, L. Bolondi and M. Negrini, *Oncogene*, 2008, **27**, 5651–5661; (*b*) K. A. O'Donnell, E. A. Wentzel, K. I. Zeller, C. V. Dang and J. T. Mendell, *Nature*, 2005, **435**, 839–843; (*c*) Y. Murakami, T. Yasuda, K. Saigo, T. Urashima, H. Toyoda, T. Okanoue and K. Shimotohno, *Oncogene*, 2006, **25**, 2537–2545.

9 (*a*) P. Mukhopadhyay, M. Rajesh, G. Hasko, B. J. Hawkins, M. Madesh and P. Pacher, *Nat. Protoc.*, 2007, **2**, 2295–2301; (*b*) R. R. Deng, X. J. Xie, M. Vendrell, Y. T. Chang and and X. Liu, *J. Am. Chem. Soc.*, 2011, **133**, 20168–20171.

10 (*a*) H. F. Dong, L. Ding, F. Yan, H. X. Ji and H. X. Ju, *Biomaterials*, 2011, **32**, 3875–3882; (*b*) Y. Geng, D. J. Lin, L. J. Shao, H. X. Ju and F. Yan, *PLoS One*, 2013, **8**, e65540; (*c*) H. F. Dong, J. P. Lei, H. X. Ju, F. Zhi, H. Wang, W. J. Guo, Z. Zhu and F. Yan, *Angew. Chem., Int. Ed.*, 2012, **51**, 4607–4612; (*d*) R. C. Qian, L. Ding and H. X. Ju, *J. Am. Chem. Soc.*, 2013, **135**, 13282–13285; (*e*) R. C. Qian, L. Ding, L. W. Yan, M. F. Lin and H. X. Ju, *J. Am. Chem. Soc.*, 2014, **136**, 8205–8208.

11 (*a*) X. M. Sun and Y. D. Li, *Angew. Chem., Int. Ed.*, 2004, **43**, 597–601; (*b*) L. R. Kong, X. F. Lu, X. J. Bian, W. J. Zhang and C. Wang, *Langmuir*, 2010, **26**, 5985–5990.

12 (*a*) C. H. Lu, H. H. Yang, C. L. Zhu, X. Chen and G. N. Chen, *Angew. Chem., Int. Ed.*, 2009, **48**, 4885–4887; (*b*) S. J. He, B. Song, D. Li, C. F. Zhu, W. P. Qi, Y. Q. Wen, L. H. Wang, S. P. Song, H. P. Fang and C. H. Fan, *Adv. Funct. Mater.*, 2010, **20**, 453–459; (*c*) S. S. Chou, M. De, J. Luo, V. M. Rotello, J. Huang and V. P. Dravid, *J. Am. Chem. Soc.*, 2012, **134**, 16725–16733; (*d*) Y. Wang, Z. H. Li, D. H. Hu, C. T. Lin, J. H. Li and Y. H. Lin, *J. Am. Chem. Soc.*, 2010, **132**, 9274–9276.

13 (*a*) H. L. Li, Y. W. Zhang, T. S. Wu, S. Liu, L. Wang and X. P. Sun, *J. Mater. Chem.*, 2011, **21**, 4663–4668; (*b*) R. H. Yang, J. Y. Jin, Y. Chen, N. Shao, H. Z. Kang, Z. Y. Xiao, Z. W. Tang, Y. R. Wu, Z. Zhu and W. H. Tan, *J. Am. Chem. Soc.*, 2008, **130**, 8351–8358.

14 (*a*) K. Kogure, R. Moriguchi, K. Sasaki, M. Ueno, S. Futaki and H. Harashima, *J. Controlled Release*, 2004, **98**, 317–323; (*b*) C. P. Leamon, M. A. Parker, I. R. Vlahov, L. C. Xu, J. A. Reddy, M. Vetzel and N. Douglas, *Bioconjugate Chem.*, 2002, **13**, 1200–1210.

15 (*a*) Z. Liu, J. T. Robinson, X. M. Sun and H. J. Dai, *J. Am. Chem. Soc.*, 2008, **130**, 10876–10877; (*b*) Z. Liu, S. Tabakman, K. Welsher and H. J. Dai, *Nano Res.*, 2009, **2**, 85–120.

16 X. Y. Yang, X. Y. Zhang, Z. F. Liu, Y. F. Ma, Y. Huang and Y. J. Chen, *J. Phys. Chem. C*, 2008, **112**, 17554–17558.

17 M. Zuker, *Nucleic Acids Res.*, 2003, **31**, 3406–3415.

18 H. F. Dong, J. Zhang, H. X. Ju, H. T. Lu, S. Y. Wang, S. Jin, K. H. Hao, H. W. Du and X. J. Zhang, *Anal. Chem.*, 2012, **84**, 4587–4593.

19 Y. R. Wu, J. A. Phillips, H. P. Liu, R. H. Yang and W. H. Tan, *ACS Nano*, 2008, **2**, 2023–2028.

20 J. R. Casey, S. Grinstein and J. Orlowski, *Nat. Rev. Mol. Cell Biol.*, 2010, **11**, 50–61.

21 D. Fischer, T. Bieber, Y. Li, H. P. Elsässer and T. Kissel, *Pharm. Res.*, 1999, **16**, 1273–1279.

22 A. K. Varkouhi, M. Scholte, G. Storm and H. J. Haisma, *J. Controlled Release*, 2011, **150**, 220–228.

23 M. Huang, C. W. Fong, E. Khor and L. Y. Lim, *J. Controlled Release*, 2005, **106**, 391–406.

24 B. R. Cullen, *Mol. Cell*, 2004, **16**, 681–865.

25 J. Panyam, W. Z. Zhou, S. Prabha, S. K. Sahoo and V. Labhasetwar, *FASEB J.*, 2002, **16**, 1217–1226.

26 Y. Lu, J. M. Thomson, H. Y. Wong, S. M. Hammond and B. L. Hogan, *Dev. Biol.*, 2007, **310**, 442–453.

